ELSEVIER

Fusion Engineering and Design 28 (1995) 699–707

Fusion Engineering and Design

Calorimetric measurements of nuclear heating in small probes of plasma-facing materials

A. Kumar [a], Y. Ikeda [b], M.A. Abdou [a], M.Z. Youssef [a], C. Konno [b], K. Kosako [b], Y. Oyama [b], T. Nakamura [b], H. Maekawa [b]

[a] *School of Engineering and Applied Science, University of California at Los Angeles, Los Angeles, CA 90024, USA*
[b] *Department of Reactor Engineering, Japan Atomic Energy Research Institute, Tokai, Ibaraki 319-11, Japan*

Abstract

Total nuclear heating rates have been measured in simulated D–T fusion neutron environment under a USDOE–JAERI collaborative program. An automated, microcalorimetric technique was developed for on-line measurements of total nuclear heating in a mixed neutron plus photon field. Irradiated probe materials included graphite, titanium, stainless steel 304, molybdenum, and tungsten, among others. Analysis of the measurements has revealed large deviations between calculations and experiments. An approach based on sensitivity theory is sketched for estimating uncertainty on total nuclear heating. Also, we observe that calculation-to-experiment (CE) ratio data for all libraries and materials can be consolidated to obtain a probability density distribution of CE ratios that roughly resembles a gaussian distribution centred at 1.04.

1. Introduction

It has long been recognized that reliable prediction of nuclear heating in a fusion reactor is one of the most critical issues confronting a designer. Elaborate methodologies have been provided time and again to compute kerma factors and create their libraries [1–6]. However, until recently, practically no experimental data had been available on nuclear heat deposition rates, in a D–T neutron field, to test the kerma factor libraries. An extensive, experimental program of total nuclear heating measurements was launched within the framework of a USDOE–JAERI collaborative program in 1988 [7–10]. This effort culminated in 1993 [7–10]. It was required to develop a sophisticated technique to measure very low temperature changes produced in a mixed neutron and photons field produced by a limited number of D–T neutrons. The source neutron intensity hovered around 3×10^{12} n s^{-1}, and a typical calorimetric probe was kept at a distance of about 4 cm to enhance the signal for measurement purposes [7–10].

A number of materials under consideration for ITER, i.e. molybdenum, tungsten, titanium, graphite (plasma-facing components), copper (magnet coils), iron, stainless steel, nickel (structural material components), aluminum etc., were chosen for experiments. However, at present, we will be dealing with measurements made on plasma-facing materials only, including graphite, titanium, copper, zirconium, niobium, molybdenum, tin, tungsten, and lead. For almost all of these materials, the ratio of calculation to experimental (CE)

0920-3796/95/$09.50
SSDI 0920-3796(94)00321-1

measurement shows a large dispersion as one compares various kerma factor libraries. Interestingly, CE data for all libraries and materials can be consolidated to obtain a probability density distribution of CE ratios that very much resembles a gaussian distribution centered at 1.04. We define and elaborate on the concept of "quality factor" for total nuclear heating. This factor helps in qualitatively understanding the status of uncertainty involved in predicting total nuclear heating in different materials using currently available kerma factor libraries.

2. Calorimetric experiments for total nuclear heating measurements

Extensive experiments on total nuclear heating were planned and executed under a USDOE–JAERI collaborative program on fusion neutronics [7–10]. The experimental geometry and other details for a majority of the experiments are already available [7–10]. A microcalorimetric technique employing small probes of various materials was developed and applied for direct measurement of total nuclear heating, deposited by neutrons and induced photons. On-line data acquisition and treatment were applied to obtain nuclear heat deposition rates in probes of various materials, a typical probe measuring 2 cm in diameter by 2 cm in length, of graphite, aluminum, titanium, iron, stainless steel 304, copper, nickel, zirconium, niobium, molybdenum, tin, tungsten, lead, and lithium carbonate. Typically, a probe was kept at a distance of about 4–8 cm from the rotating neutron target with a nominal intensity of about 3×10^{12} n s^{-1}. The microcalorimeters were subjected to spaced neutron pulses of 3–10 min duration.

Bead thermistors and platinum resistance temperature detectors were employed as thermal sensors within calorimeters made of single materials (or probes). The first experiments were conducted during June 1989 and the tested materials included Fe, Al, C, Cu. Each of these calorimeters was placed inside a vacuum chamber and the mean distance from the target was about 8 cm. The measured heat deposition rates ranged from 7 to 30 μW g^{-1} for a normalized source strength of 10^{12} n s^{-1}. The experiments were carried out again in December 1989. This allowed us to verify the reproducibility. The average target–probe distance was shortened to about 5 cm, which led to 2–3 times higher rates. Tungsten was also included. Later, during November 1990 and October–November 1991, experimental measurements were done on small single probes of graphite, titanium, stainless steel 304, nickel, zinc, zirconium, niobium, molybdenum, tin, tungsten, lead, and lithium carbonate. Typical distance from target to probe was narrowed down to about 3.7 cm. Raw resistance change data measured for various thermal sensors sitting inside an evacuated microcalorimeter that was exposed to neutron pulses were treated to obtain eventually total nuclear heat deposition rate in the micro-calorimeter medium.

3. Comparison of calculation with experimental measurements

The three-dimensional code MCNP [11] was used for modeling the experimental geometry. The RMCCS library was used for neutron interactions and photon production in the whole system. This library has many cross-sections based on ENDF/B-V. Particle transport computations were repeated with the ENDL85 library and differences were seen between neutron–photon energy spectra evaluated by the two libraries. Heating numbers from four libraries available [11] with MCNP, i.e. BMCCS, ENDL85, RMCCS, ENDF5T (or ENDF5U), were used for a comparison of nuclear heating rates. It is to be noted that ENDF5T–ENDF5U, and RMCCS, to large extent, originated from ENDF/B-V; ENDL85 was the latest library available from Lawrence Livermore National Laboratory; BMCCS contained older data, i.e. from ENDF/B-IV or ENDL73 files. RMCCS, ENDF5T–ENDF5U, and BMCCS (if from ENDF/B-IV) libraries contain heating numbers obtained by "direct energy balance" method [4,12,13]. Some of these heating numbers have been known to be negative owing to inconsistencies in evaluated nuclear data for a number of isotopes [4,12,13]. ENDL85 has positive heating numbers that are used to adjust photon production cross-sections and spectra for self-consistency [4,13]. MCPLIB was utilized for photon interactions and transport. Nuclear heat deposition rate was averaged over the volume of a probe, and then converted to temperature change rate, using specific heat data from Ref. [14].

In addition to the libraries available with MCNP, we have also used various other kerma factor libraries to obtain neutron and γ ray (or photon) heating rates, using RMCCS-calculated neutron photon spectra for each experiment. The ENDF/B-VI-based MATXS library MATXS10, and ENDF/B-V-based MATXS library, MATXS5, are among those libraries [5,15]. Each library has 30 neutron groups and 12 photon groups [15]. In fact, there are two versions each for these two libraries, e.g. MATXS10-HEAT, MATXS10-KERMA, MATXS5-HEAT, and MATXSF-KERMA. The "HEAT" index stands for neutron

kerma factors obtained through a direct energy balance method [5,16]. The KERMA index stands for "kinetic upper-estimate kerma" [5,16]. It is expected that the HEAT kerma factor should generally be smaller than or equal to the corresponding KERMA value [16]. In a small system, one could expect considerable differences between the heating rates using HEAT and KERMA versions of a MATXS library, as a good part of the energetic photons could escape from it.

Among other kerma factor libraries, KAOSLIB [4], a new kerma factor library generated from ENDF/B-V library using KAOS-V code [4], and a JENDL-3-based library were also used. In fact, we have used two variations of KAOSLIB library: (1) KAOSLIB-REC, "recommended" version, and (2) KAOSLIB-REC + CPD, "recommended plus charged particle decay heat" version. The latter variation includes decay heats from all radioactive charged particle products (or, in other words, recoiling products that are radioactive too) having half-lives up to 1 day. The JENDL-3-based library [17,18] has 125 neutron groups and it was obtained from basic JENDL-3 data files using NJOY processing code, and the photon kerma factors came from DCL-99 [19]. To minimize the sources of discrepancies, we have adopted the photon heating rates calculated with the RMCCS library for all the libraries being compared.

3.1. Calculation-to-experiment ratio trends

In what follows, we are presenting CE results using different kerma factor libraries for only selected materials. The materials include graphite, titanium, copper, molybdenum, and lead. We have assigned an average of 10% error to each experimental value.

3.1.1. Graphite

Nuclear heating measurements were made with graphite single probes during experimental periods of June 1989 (A), December 1989 (B), November 1990 (C), and October–November 1991 (D). As shown in Fig. 1, CE ratios for graphite range from 1.14 (MATXS10) to 1.36 (BMCCS). BMCCS overprediction can be ascribed to largest neutron kerma factors for this library in the important energy region above 10 MeV. The kerma factors have a very strong dependence on neutron energy: the kerma factor is about 2×10^{-13} J b close to 10 MeV and drops by five orders of magnitude to about 10^{-18} J b as the neutron energy drops by six orders of magnitude to 10^{-5} MeV. There is a region of large differences between about 3 and about 10 MeV. MATXS10-HEAT and ENDL-85 are generally close to each other. JENDL-3 kerma factors are systematically lower

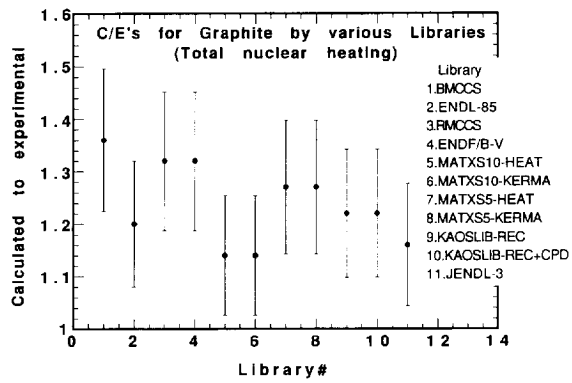

Fig. 1. Graphite: CE ratio for total nuclear heating, as a function of kerma factor library. Libraries include BMCCS, ENDL-85, RMCCS, ENDF/B-V, MATXS10, MATXS5, KAOSLIB, and JENDL-3.

than those from MATXS10-HEAT in the energy range from about 10 to about 13 MeV, but the trend reverses above about 14 MeV. MATXS5-HEAT kerma factors are close to those from MATXS10-HEAT except above 15 MeV. In the topmost energy group, from 15 to 17 MeV, the kerma factor in the former is almost 20% larger than that in the latter.

3.1.2. Titanium

Nuclear heating measurements were made with titanium single probes during experimental periods of November 1990 (C) and October–November 1991 (D). As shown in Fig. 2, CE ratios for titanium range from 0.62 (KAOSLIB-REC) to 1.41 (MATXS10-KERMA). It appears that this large variation is mostly attributable to

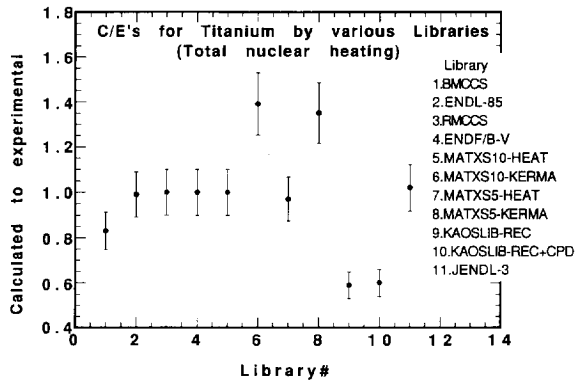

Fig. 2. Titanium: CE ratio for total nuclear heating, as a function of kerma factor library. Libraries include BMCCS, ENDL-85, RMCCS, ENDF/B-V, MATXS10, MATXS5, KAOSLIB, and JENDL-3.

large differences in neutron kerma factors for different libraries. JENDL-3 and ENDL-85 kerma factors appear to be close above 9 MeV. MATXS10-HEAT and ENDL-85 kerma factor curves cross around 12 MeV and 15 MeV, and below 10 MeV the difference between them rises. MATXS10-KERMA values are as much as 30%–50% higher than those from MATXS10-HEAT in the energy range above 8 MeV. KAOSLIB kerma factors show very odd behavior. In fact, the kerma factors from this library start to decline beginning at 12 MeV and rise again at 15 MeV, whereas, for all other libraries, the kerma factors continue to rise between 12 and 17 MeV.

3.1.3. Copper

Measurements were made with copper single probes during experimental periods of June 1989 (A) and December 1989 (B). As shown in Fig. 3, CE ratios for copper range from 0.77 (RMCCS–ENDF5) to 1.54 (KAOSLIB-REC + CPD). This large variation is due to large differences in neutron kerma factors for different libraries. JENDL-3 and ENDL-75 kerma factors are close above about 0.2 MeV. RMCCS values oscillate a lot about the ENDL-85 curve. Surprisingly, RMCCS hits a peak around 10–12 MeV and then drops precipitously between 13.5 and 15 MeV. MATXS5-HEAT oscillates around ENDL-85 and even turns negative around 1.5 MeV.

3.1.4. Molybdenum

The nuclear heating measurements were made with single molybdenum probes during experimental periods of November 1990 (C), and October–November 1991 (D). As shown in Fig. 4, CE ratios for molybdenum range from 0.71 (MATXS10-HEAT, MATXS5-HEAT) to 1.08 (JENDL-3). This variation is attributable to very large

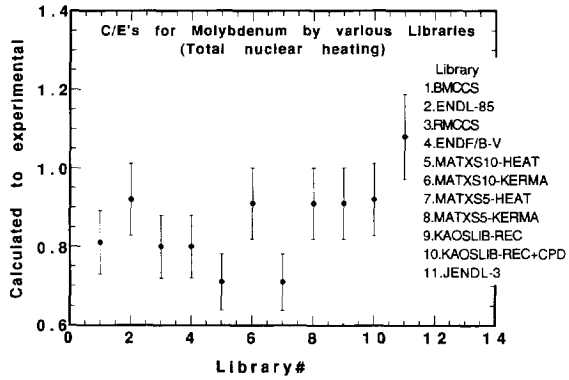

Fig. 4. Molybdenum: CE ratio for total nuclear heating, as a function of kerma factor library. Libraries include BMCCS, ENDL-85, RMCCS, ENDF/B-V, MATXS10, MATXS5, KAOSLIB, and JENDL-3.

differences in neutron kerma factors for different libraries. MATXS10-KERMA and ENDL-85 kerma factors appear to be quite close. JENDL-3 stays around ENDL-85 from about 10^{-2} through about 1 MeV, and is considerably below ENDL-85 between 2 and 3 MeV. It rises rapidly and overtakes ENDL-85 and is significantly larger at 6 MeV. Above 12 MeV, JENDL-3 kerma is much higher. RMCCS and MATXS10-HEAT kerma factors oscillate wildly. RMCCS kerma drops to zero between 15 and 13.5 MeV. MATXS10-HEAT stays continuously negative from 17 to 7.8 MeV.

3.1.5. Lead

Nuclear heating measurements were made with lead single probes during the experimental period of October–November 1991 (D). As shown in Fig. 5, CE ratios

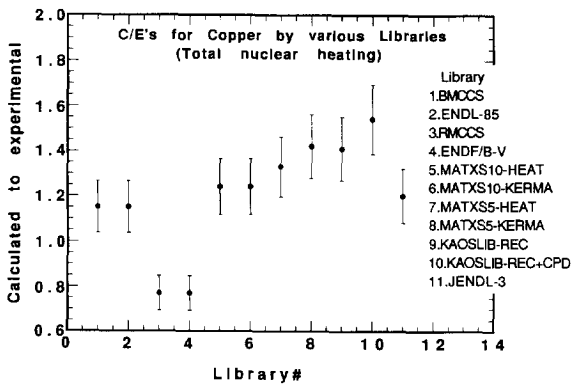

Fig. 3. Copper: CE ratio for total nuclear heating, as a function of kerma factor library. Libraries include BMCCS, ENDL-85, RMCCS, ENDF/B-V, MATXS10, MATXS5, KAOSLIB, and JENDL-3.

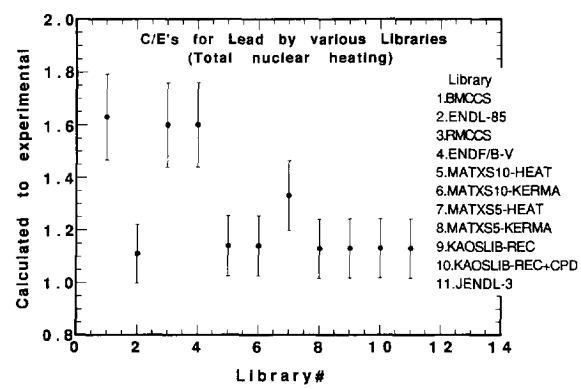

Fig. 5. Lead: CE ratio for total nuclear heating, as a function of kerma factor library. Libraries include BMCCS, ENDL-85, RMCCS, ENDF/B-V, MATXS10, MATXS5, KAOSLIB, and JENDL-3.

for lead range from 1.1 (ENDL-85–MATXS5-KERMA) to 1.6 (RMCCS–BMCCS–ENDF5). This large variation is mostly attributable to large differences in neutron kerma factors for different libraries, as photon heating is taken to be identical. The libraries with the largest CE ratios are those that have abnormally large neutron heating fractions. For example, BMCCS (CE ratio, 1.63), RMCCS (CE ratio, 1.60), and ENDF5 (CE ratio, 1.60), have rather large, fractional neutron heating values of 0.35, 0.34, and 0.34 respectively. On the contrary, ENDL-85, MATXS10-HEAT (CE ratio, 1.14), and MATXS10-KERMA (CE ratio, 1.14) have low, fractional neutron heating values of 0.050, 0.059, and 0.059 respectively. ENDL-85, MATXS10-HEAT, and JENDL-3 kerma factors are close to one another. RMCCS and MATXS5-HEAT kerma factors show large deviations from the other three. Additionally, MATXS5-HEAT kerma factors are negative for many energy groups above 2 MeV. RMCCS kerma factors show oscillatory behavior above 2 MeV. RMCCS kerma factors are almost the largest above 10 MeV. Interestingly, the RMCCS value peaks for the 15–13.5 MeV group and decreases on either side of this group, and this peak value is more than an order of magnitude larger than that for any other library.

4. Contributors to disagreement between calculation and measurement

In principle, both the calculation and measurement carry uncertainty.

4.1. Experimental factors

There are a number of factors that contribute to experimental error: positioning of microcalorimeter relative to D–T neutron source, source neutron intensity, determination of net temperature derivative from resistance drift curve, and specific heat of the probe. The total uncertainty is estimated to vary from about 6% to about 12% for the measurements made so far under the collaborative program.

4.2. Calculational factors

Let us understand the roles of a kerma factor, say $k(E)$, and radiation (neutron–γ ray) spectrum, say $\Phi(E)$, in contributing to total nuclear heating rate, say H, expressed as follows:

$$H = \int_0^{\infty} \Phi(E)k(E)\,\mathrm{d}E = \sum_{i=1}^{n+g} \Phi_i k_i\,\Delta u_i = \sum_{i=1}^{n+g} \Phi_i (\mathrm{KI})_i \quad (1)$$

Here $(\mathrm{KI})_i$ is used to define another useful quantity KI as follows:

$$\mathrm{KI} = \sum_{i=1}^{n+g} (\mathrm{KI})_i = \sum_{i=1}^{n+g} k_i\,\Delta u_i \quad (2)$$

The subscript represents the ith energy group out of a total of $n+g$ groups, where n and g are the numbers of neutron and γ ray energy groups. Φ_i is the radiation energy spectrum in energy group i and is defined per unit lethargy. Δu_i is net lethargy change for group i. KI stands for "kerma factor integral". Ideally, there should be a very large number of energy groups so as to describe accurately the fine features of both the kerma factors and the radiation spectra. In reality, one is forced to restrict the number of energy groups. If the number of energy groups is low or the energy group boundaries are inappropriately chosen, one would have a significant contribution to the uncertainty on H from this source alone. The maximum uncertainty in H can be expressed as

$$\left|\frac{\Delta H}{H}\right|_{\max} = \sum_{i=1}^{n+g} |S_i\,\Delta u_i| \left(\left|\frac{\Delta k_i}{k_i}\right| + \left|\frac{\Delta \Phi_i}{\Phi_i}\right| \right) \quad (3)$$

where S_i is to be understood as the differential sensitivity for energy group i and is given as

$$S_i = \frac{\Phi_i k_i}{\sum_{j=1}^{n+g} \Phi_j k_j\,\Delta u_j} \quad (4)$$

It follows from Eq. (3) that one needs to have relative uncertainties $|\Delta k_i/k_i|$ and $|\Delta\Phi_i/\Phi_i|$ on kerma factor as well as spectrum in addition to the differential sensitivity profile, say S_i, to determine the relative uncertainty on the nuclear heating rate H.

Fig. 6 compares differential sensitivity profiles for total nuclear heating as a function of neutron and γ ray energy for a probe of molybdenum. The peak sensitivity, to the neutron contribution, has a value of about 0.7 for 15–13.5 MeV for ENDL-85. The sensitivity for ENDL-85 averages about 2×10^{-3} in a relatively flat region extending from 10 to 0.5 MeV, and thereafter it drops continuously. The largest γ sensitivity value of about 0.4 occurs between 6 and 5 MeV, and it is almost a factor of 2 lower than the largest neutron sensitivity. The strong component of photon heating to total nuclear heating is evident for molybdenum. Fig. 7 shows relative deviation in neutron and γ ray spectra for a probe of molybdenum. The spectra for neutrons and photons were obtained by doing two MCNP calculations with the same model, but with two transport cross-section libraries, i.e. RMCCS and ENDL-85. One can notice a 20%–40% deviation with respect to the mean spectra.

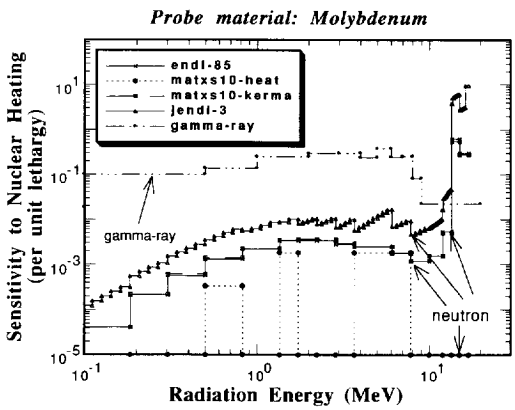

Fig. 6. Total nuclear heating differential sensitivity profiles as a function of neutron and γ ray energy for a molybdenum probe under D–T neutron irradiation.

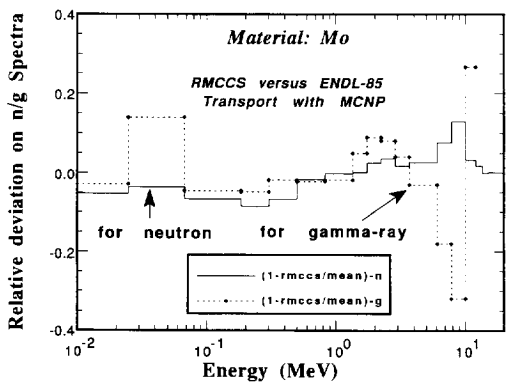

Fig. 7. Relative deviation of neutron and γ ray spectra with respect to their means for a molybdenum under D–T neutron irradiation.

Fig. 8 provides an example of differences in neutron kerma factors for molybdenum. Note that, kerma factors predicted by MATXS10-HEAT library oscillate wildly and turn negative at will.

5. Probability distribution of calculation-to-experiment ratios

It is clear from the previous sections that there is significant disagreement between calculation and experiment for almost all the materials. The inadequacies in radiation (neutron–photon) transport cross-sections, methodology of transport solver, and geometrical–material modeling of the irradiated assembly are notable

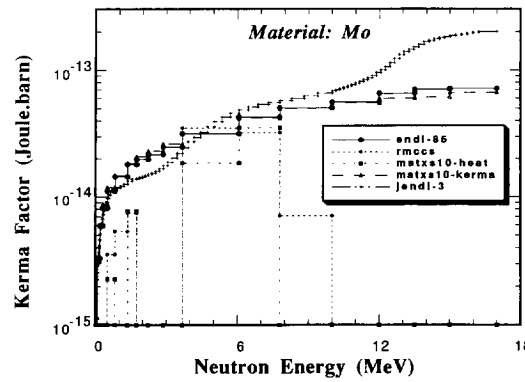

Fig. 8. Neutron kerma factors for molybdenum as included in various libraries.

contributors to uncertainties in calculated spectra. The designers of a fusion machine need reliable information on total nuclear heating in its various components. However, it is a task that is made even more formidable by the complexity of the underlying physics. All neutron-induced reactions command interest. It is to be remembered that (n, γ) reactions are preferably provoked by the low energy part of the neutron energy spectrum, unlike (n, 2n), (n, p), (n, np–d), (n, t), (n, α) reactions that are preferably provoked by the high energy part of the spectrum. The neutron kerma factors fall rapidly as the neutron energy drops. Thus, most of the contribution of the neutron component of total nuclear heating comes from the hardest part of the spectrum. However, even a small fraction of low energy neutrons could lead to sizeable production of photons through the (n, γ) reaction, which might, in turn, lead to a relatively significant amount of photon heating, even for a machine component close to the D–T plasma.

5.1. Quality factor

The designers acknowledge the inadequacies of modeling and cross-section data, and incorporate safety factors to come up with a somewhat conservative design [20,21]. Sizeable underprediction or overprediction of nuclear heating by calculation is undesirable owing to its implications for large overheating or underheating of localized spots in a fusion machine. Ideally, one needs to correct the calculation, using a multiplier, such that the corrected prediction is equal to actual (experimental) amount of total nuclear heating. This correction factor for a code (and library) can be defined as

ideal corrective multiplier (ICM) = 1/(CE ratio)

where the inverse of the observed CE ratios defines the correction factor ICM for a given material. As long as one has access to very large amount of CE data for each material, one can obtain the ICM and associated confidence level. For example, for nuclear heating, ICM can also be seen as a quality factor that is indicative of the quality of the ensemble of transport cross-sectional library, photon production cross-sections, computed neutron and photon spectra, neutron and photon kerma factors, and experimental data.

In practice, it is almost impossible to obtain the ICM as defined above owing to problems associated with (i) impossibility of exact modeling of the experimental assembly, (ii) non-vanishing errors of the calculational method–code, and (iii) finite experimental error. Thus, one will rather be dealing with a distribution of correction factors. If this distribution is statistically reliable, one can set a confidence level and obtain a correction factor which, when multiplied by the calculated value, yields a corrected calculational result that will be equal to or greater than the experimental value for ensuring overprediction, or the reverse if underprediction of total nuclear heating will be required. Such a multiplier could be called a safety factor or a quality factor. Mathematical formulation and a procedure to obtain the probability density distribution function of the CE ratio, quality factor (safety factor), and associated confidence level are described elsewhere [22].

5.2. Probability density distribution function

A designer could be interested in ascertaining the quality of a kerma factor library. In principle, a separate quality factor can be associated with each library if all other parameters are held constant. One can obtain a probability density distribution of CE ratios, irrespective of probe material, neutron or photon energy spectrum. Theoretically, the CE ratio could vary from 0 to ∞. It is useful to define another variable y, such that

$$y = 1 + \log(\text{CE ratio})$$

and

$$\text{CE ratio} = \exp(y - 1)$$

y will vary from $-\infty$ to $+\infty$, for CE ratio varying from 0 to $+\infty$. There are two advantages in doing this transformation: (i) one practically contracts the independent variable space, and (ii) one can directly compare such a probability density distribution with a gaussian distribution. First of all, let us look at the shape of a consolidated probability density distribution of CE ratios. Fig. 9 shows a plot of a consolidated

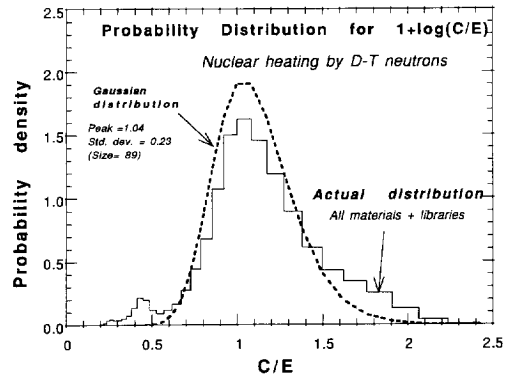

Fig. 9. Probability density of CE ratios, expressed as a function of $y = 1 + \log(\text{CE ratio})$, for total nuclear heating produced by D–T neutrons, for various materials and kerma factor libraries.

probability density distribution for $1 + \log(\text{CE ratio})$, as a function of CE ratio. Also plotted is a gaussian distribution. Although the actual probability density distribution is deceptively similar to the gaussian distribution, one can observe significant differences in the two on either side of the peak. On lower end of CE ratios one can, in fact, notice a secondary peak in the CE ratio range from 0.4 to 0.5. Zirconium and, to some extent, titanium contribute predominantly to this secondary peak. On the higher end of CE ratios, one notices a rising discrepancy between the two distributions beyond 1.5. Lead, zirconium and, to some extent, copper and titanium contribute to this discrepancy. Fig. 10 shows fractional confidence level as a function of quality factor for various kerma factor libraries. We

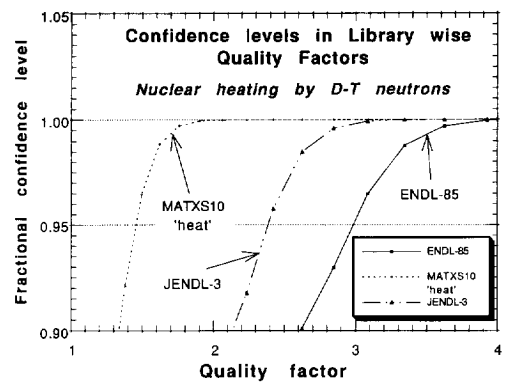

Fig. 10. Library-wise fractional confidence level as a function of quality factor, for ENDL-85, MATXS10-HEAT, and JENDL-3 libraries, using individual probability density distributions for each library.

observe that, for a confidence level above 90%, the quality factors will have the following ascending order for these libraries: MATXS10-HEAT, JENDL-3, and ENDL-85. The quality factors range from 1.4 to 2.6. The lowest quality factor of 1.4 applies both to MATXS10-HEAT and to MATXS5-HEAT. This means that, if one were to use either of these two libraries for any of the nine materials, the calculated heating rate would have to be multiplied by 1.4 to ensure that the modified heating rate carries 90% confidence level. The largest quality factor of 2.6 is obtained for ENDL-85. The very low CE ratio (0.34) for zirconium given by ENDL-85 is largely responsible for such a high quality factor for ENDL-85.

6. Conclusions

The USDOE–JAERI collaboration on nuclear heating experiments has brought out large disagreements between calculations and measurements for almost all the probe materials. The responsible factors include kerma factors, spectra (neutron and/or photon), methodology and assumptions characterizing transport solver, calculational model, and experimental errors. The CE ratio results from different libraries were processed to obtain probability density distribution functions, confidence levels and quality factors for prediction of total nuclear heating in a D–T neutron environment.

Acknowledgements

The US contribution was supported by the US Department of Energy, Office of Fusion Energy, under Contract DE-FG03-86ER52123.

References

[1] M.A. Abdou and C.W. Maynard, Calculational methods for nuclear heating—part I: theoretical and computational algorithms, Nucl. Sci. Eng. 56 (1975) 360.

[2] M.A. Abdou and C.W. Maynard, Calculational methods for nuclear heating—part II: applications to fusion-reactor blankets and shields, Nucl. Sci. Eng. 56 (1975) 381.

[3] M.A. Abdou, C.W. Maynard and R.Q. Wright, MACK: a computer program to calculate neutron energy release parameters (fluence-to-kerma factors) and multigroup reaction cross sections from nuclear data in ENDF format, Oak Ridge National Laboratory Rep. ORNL-TM-3994, July 1973.

[4] Y. Farawila, Y. Gohar and C. Maynard, KAOS-V code: an evaluation tool for neutron kerma factors and other nuclear responses, Argonne National Laboratory Rep. ANL/FPP/TM-240, September 1989; KAOS/LIB-V: a library of nuclear response functions generated by KAOS-V code from ENDF/B-V and other data files, Argonne National Laboratory Rep. ANL/FPP/TM-241, April 1989.

[5] R.E. MacFarlane, D.W. Muir and R.M. Boicourt, The NJOY nuclear data processing system, volume II: the NJOY, RECONR, BROADR, HEATR, and THERMR modules, Los Alamos National Laboratory Rep. LA-9303-M, Vol. II (ENDF-324), May 1982.

[6] R.S. Caswell and J.J. Coyne, Kerma factors for neutron energies below 30 MeV, Radiat. Res. 83 (1980) 217.

[7] A. Kumar, M.A. Abdou, Y. Ikeda and C. Konno, Radioactivity and nuclear heating measurements for fusion applications, in B.E. Keen, M. Huguet and R. Hemsworth (eds.), Fusion Technology 1990, Elsevier, Amsterdam, 1991, pp. 872–876.

[8] A. Kumar, Y. Ikeda and C. Konno, Experimental measurements and analysis of nuclear heat deposition rates in simulated d–t neutron environment: JAERI/USDOE collaborative program on fusion neutronics experiments, Fusion Technol. 19 (1991) 1979.

[9] A. Kumar, M.Z. Youssef, M.A. Abdou, Y. Ikeda, C. Konno, K. Kosako, Y. Oyama and T. Nakamura, Direct nuclear heating measurements in fusion neutron environment and analysis, Fusion Eng. Des. 18 (1991) 397.

[10] Y. Ikeda, C. Konno, K. Kosako, Y. Oyama, F. Maekawa, H. Maekawa, A. Kumar, M.Z. Youssef and M.A. Abdou, Measurement and analysis of nuclear heat deposition in structural materials induced by d–t neutrons, Fusion Technol. 21 (1991) 2190.

[11] J.F. Briesmeister (ed.), MCNP—a general Monte Carlo code for neutron and photon transport: version 3A, Rep. LA-7396-M, Rev. 2, September 1988; MCNP3B Newsl. July 18, 1988 (Los Alamos National Laboratory).

[12] R. Little and R. Seamon, Negative heating numbers, Los Alamos National Laboratory Memo. to P. Young and E. Arthur, CSEWG Evaluations Committee, June 17, 1981.

[13] R. MacFarlane, Energy balance of ENDF/B-V, Trans. Am. Nucl. Soc. 33 (1979) 681.

[14] Y.S. Touloukian and E.H. Buyco, Specific Heat: Metallic Elements and Alloys, Series on Thermophysical Properties of Matter, Vol. 4, IFI–Plenum, New York, 1970; Specific Heat: Nonmetallic Solids, Series on Thermophysical Properties of Matter, Vol. 5, IFI–Plenum, New York, 1970.

[15] R.E. MacFarlane, TRANSX-CTR: a guide for interfacing MATXS cross-section libraries to nuclear transport codes for fusion systems analysis, Los Alamos National Laboratory Rep. LA-9863-MS, February 1984.

[16] R.E. MacFarlane, Personal communication, October 1993.

[17] K. Shibata, T. Kakagawa, T. Asami et al., Japanese evaluated nuclear data library, version-3, JAERI-1319, 1990.
[18] K. Maki, K. Kosako, Y. Seki and H. Kawasaki, Nuclear group constant set FUSION-J3 for fusion reactor nuclear caclulations based on JENDL-3, JAERI-M91-072, 1991.
[19] R.W. Roussin, J.R. Knight, J.H. Hubbell and R.J. Howerton, Description of DLC99/HUGO package of photon interaction data in ENDF/B-V format, ORNL/RSIC-46 (ENDF-335), 1983.
[20] M.E. Sawan and L.A. El-Guebaly, Three-dimensional neutronics analysis for the US magnet shield of ITER, Fusion Technol. 19 (1991) 1469.
[21] L.A. El-Guebaly, Overview of the US-ITER magnet shield: concept and problems, Fusion Technol. 19 (1991) 1475.
[22] A. Kumar, Y. Ideda, M.A. Abdou, M.Z. Youssef, C. Konno, K. Kosako, Y. Oyama, T. Nakamura and H. Maekawa, Measurements of D–T neutron induced radioactivity in plasma facing materials and their role in qualification of activation cross-section libraries and codes, Fusion Eng. Des. 28 (1995).